Organic & Biomolecular Chemistry

Electronic Effects of Conjugated Aryl Groups on the Properties and Reactivities of Di(arylethynyl)tetracenes

Journal:	*Organic & Biomolecular Chemistry*
Manuscript ID	OB-ART-10-2023-001601.R1
Article Type:	Paper
Date Submitted by the Author:	14-Nov-2023
Complete List of Authors:	Yan, Yu; Tufts University, Chemistry Brega, Valentina; Tufts University, Chemistry Pina, Manuel; Tufts University, Chemistry Thomas, Samuel; Tufts University, Chemistry

ARTICLE

Electronic Effects of Conjugated Aryl Groups on the Properties and Reactivities of Di(arylethynyl)tetracenes

Received 00th January 20xx,
Accepted 00th January 20xx

DOI: 10.1039/x0xx00000x

Yu Yan, Valentina Brega, Manuel M. Pina, and Samuel W. Thomas III*

The photochemical oxidations of acenes can cause challenges with their optoelectronic applications, such as singlet fission and organic transistors. At the same time, these reactions form the basis for many luminescent sensing schemes for $^1O_2$. While diethynyl substitution is arguably the most widely adopted of the various substitution strategies to control oxidation and also improve solubility and processability of long acenes, the extent to which differences between the alkyne groups can influence key properties of long acenes remains largely unknown. This report therefore describes the effects of various arenes and heteroarenes on the electronic structures, optical properites, and reactivity with singlet oxygen for eight 5,12-di(arylethynyl)tetracenes. The fluorescence spectra of these tetracenes span approximately 100 nm, while their observed rate constants for reaction with singlet oxygen correlates strongly with the HOMO level, spanning one order of magnitude. They are also amenable to fluorescent materials that respond ratiometrically to singlet oxygen. Therefore, electronic effects of groups directly conjugated to ethynylacenes offer a useful chemical space for rational acene design.

Introduction

Fused polycyclic acenes are a foundational class of organic compounds in physical organic chemistry that present a unique combination of optoelectronic properties and reactivity.[1, 2] The thermodynamics of acene aromaticity influences rates and regiochemistry of their reactions, with reactivity increasing with acene length.[3-5] In addition to aromatic substitution reactions, acenes can be excellent diene reaction partners in [4+2] and [4+4] cycloaddition reactions. The cycloadditions of anthracenes, especially those with highly reactive dieneophiles and in photochemical [4+4] dimerizations have proven especially useful in various materials applications.[6-8] However, for these longer acenes with more than three fused arenes, the most important cycloadditions are with $^1O_2$ as the dieneophile to produce endoperoxides transistors and materials for singlet fission prioritize acene stability and persistence for performance in optoelectronic devices and during processing. Most acenes photosensitize $^1O_2$ efficiently and cycloadd rapidly with $^1O_2$, resulting in rapid photochemical oxidation of acenes that destroys their favorable optoelectronic properties.[9] On the other hand, our research group has leveraged these rapid endoperoxidations in responsive polymers and nanomaterials, where acene oxidation widens their frontier molecular orbital gap, preventing them from accepting energy from excited donor chromophores and yielding ratiometric fluorescence changes in response to $^1O_2$. [10-14]

Given the importance of this class of reactions, it is critical to understand how the chemical structures of acenes influences acene-$^1O_2$ reactivity. Various approaches have emerged to mitigate these photooxidations,[15] such as steric hinderance of cycloaddition,[16-18] or designing acenes that are poor sensitizers of $^1O_2$.[19, 20] However, electronic substituent effects remain highly popular, especially ethynyl substituents on acenes,[21] which can enhance acene persistence under photo-oxidative conditions. The *sp* carbon atoms are electron withdrawing and therefore make the acene less reactive as a diene in cycloadditions,[22] and additional electron withdrawing silicon atoms as in TIPS-pentacene or TIPS-anthradithiophene, and electronic substituent effects on 9,10-diethynylanthracenes also influence the oxidation rate.[23] Beyond these incremental electronic effects, ethynyl groups also stabilize anthracenes and pentacenes specifically through different mechanisms: endoperoxides of 9,10-diethynylanthracenes cyclorevert rapidly at room temperature,[24] while 6,13-diethynylpentacenes physically quench $^1O_2$, possibly through an energy transfer process from $^1O_2$ to acene-based low energy triplet states.[23]

Between these structural bookends of anthracene and pentacene, however, a range of important classes of 4- and 5-ring (hetero)acenes exist.[22, 25] Symmetrically substituted 5,12-diethynyltetracenes are the simplest structures to fall into this category, and are important in $^1O_2$-responsive polymeric materials,[26] emitters in chemiluminescence applications,[27, 28] materials for singlet fission,[20, 29-35] LEDs,[36] photocatalysts,[37] and supramolecular assemblies.[38] Therefore, our goal is to understand the extent to which electronic effects on the alkyne groups of 5,12-diethynyltetracenes influence both their electronic structures, especially their optical properties for the purposes of $^1O_2$-responsive luminescent materials, and reactivity with $^1O_2$, which is important in all applications of long

[a] *Department of Chemistry, Tufts University, Medford MA 02155 USA*
Electronic Supplementary Information (ESI) available: optical, electrochemical, and characterization data, as well as computational results and experimental section. See DOI: 10.1039/x0xx00000x

acenes. Herein, we report that electronic effects of various aryl groups on the ethynyl substituents yield both broad spectral coverage in the visible part of the spectrum as well as a 10-fold difference in rate of cycloaddition that correlates with HOMO energies.

Results and Discussion

Design and Synthesis

We targeted eight symmetrically substituted 5,12-diarylethynyltetracene derivatives, the difference between which are the aryl (Ar) groups conjugated to the ethynyl substituents. As summarized in **Chart 1**, we chose unsubstituted Ar = phenyl (**1**) as a reference compound, as well as three aryl groups typically considered electron donating (Ar = thiophene, triarylamine, and dimethylaniline) as compounds **2**-**4**, and three aryl groups typically considered electron withdrawing (Ar = pyridine, pyrazine, and benzothiadiazole) as compounds **5**-**7**. Finally, we installed Ar = tetraphenylethylene (**8**), which is known to induce aggregation induced emission (AIE),[39] to understand any impact this moiety may have on luminescence and reactivity, given our prior conclusion that rapid non-radiative decay can slow direct photo-oxidation of acenes. Compounds **4**-**8** are unreported structures, and while compounds **2** and **3** are unreported to our knowledge, they differ from previously reported compounds by only modest non-conjugated units.[36] All new compounds except for **3** were prepared by Sonogashira coupling of the corresponding aryl iodide with 5,12-diethynyltetracene, which was prepared as reported previously, while **3** was prepared by direct addition of the lithium salt of methylated 4-ethynylaniline and 5,12-tetracenequinone.

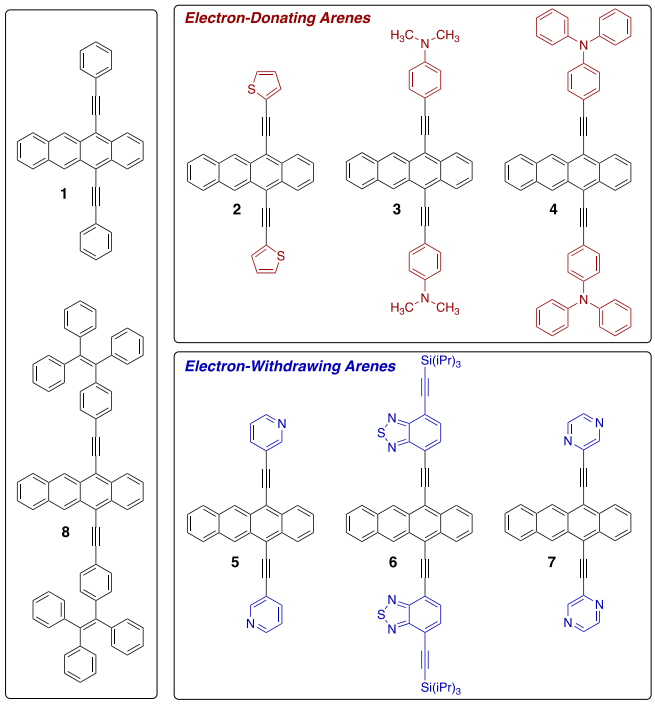

Chart 1. Structures of the eight diarylethynyltetracenes studied in this work.

Optical and Electrochemical Characterization

Figure 1 shows solution-state absorbance spectra of molecules **1**-**8**, each of which shows a strong absorbance peak in the visible range and a sharp absorbance peak in the ultraviolet. Distinct vibrational features exist in the spectra for most molecules, except **3** and **4**, each of which contain amine substitutions. Introducing potent electron withdrawing or electron donating groups and/or extending the size of the conjugated system red-shifted the absorbance maxima of these tetracenes. Among this set, molecule **6**, containing the benzothiadiazole and additional alkyne unit, shows the most red-shifted absorbance (68 nm shifted from **1**) and the highest extinction coefficient. The other two molecules with extended conjugation systems, **4** and **8**, also exhibit substantially higher extinction coefficients than the other molecules, all of which are similar.

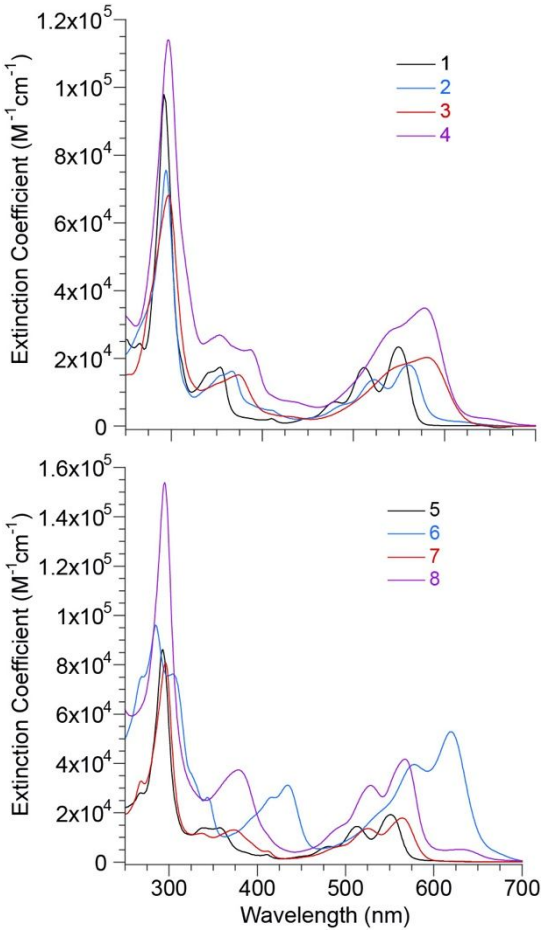

Figure 1. UV/vis absorbance spectra of **1**-**8** in chloroform.

All eight tetracenes are fluorescent with spectra spanning the yellow and orange regions of the visible spectrum (Figure 2). Like their absorbance spectra, **3** and **4** show broadened fluorescence spectra and loss of vibronic resolution at room temperature, which we attribute to the substantial electronic delocalization of the conjugated anilines into the acene chromophore, as reflected in their HOMO energies as determined electrochemically, and the electronic distributions of HOMOs and LUMOs computed by DFT (*vide infra*). Notably, **3**

has a larger red shift than the more conjugated **4**, which we attribute to a stronger electron-donating ability of dimethylaniline as opposed to triphenylamine. Again, benzothiadiazole-containing **6** has the most red-shifted spectrum, at 653 nm, 88 nm shifted from reference compound **1**, albeit with the lowest quantum yield of emission at 26%. All other molecules have quantum yields of luminescence above 50%, with triarylamine-containing **4** and pyrazine-containing **7** above 80%. We also note that, unlike its analog without triple bonds,[40] molecule **8** does not show any evidence of aggregation induced emission, as its luminescence is not substantially quenched by the tetraarylethylene unit part of the chromophore. We attribute this effect to the additional distance created by triple bonds and the lack of any distortion due to the crowded alkene not impacting the behavior of the more distant acene chromophore. Furthermore, the spectra of **3** displays positive solvatochromism in fluorescence of 23 nm (absorbance) and 56 nm (emission) between hexanes and CH_2Cl_2, indicating the strong donor-acceptor feature of this molecule due to the dimethylaniline substituents.[41, 42]

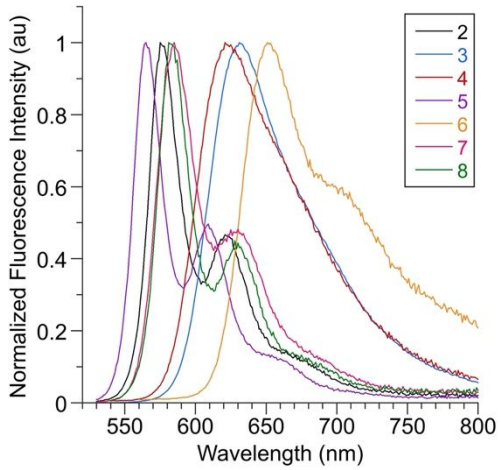

Figure 2. Fluorescence spectra of tetracenes **2-8** in chloroform.

In addition, we determined the first oxidation potentials of these molecules by cyclic voltammetry (CV). Compared with an external ferrocene reference, we calculate the energy of the highest occupied molecular orbital (HOMO) from either the peak currents during oxidation (for those molecules that show some reversibility of oxidation) or the onsets of the first oxidation peak (for those molecules that show fully irreversible oxidations), compared with the corresponding features for ferrocene. Along with theoretically computed energy levels, the results are listed in **Table 2**. In general, the molecules with electron-donating groups have elevated HOMO energies, and those with electron-withdrawing groups have lower energies. For instance, pyrazine-containing **7** shows the lowest HOMO energy at -5.4 V, while dimethylaniline-substituted **3** has the highest HOMO energy of -4.9 V, consistent with a larger electron donation character of the dimethylaniline group revealed in solvatochromism trends.

Table 1. Absorbance and fluorescence parameters of **1-8** in chloroform.

	λ_{max} (nm)	ε ($M^{-1}cm^{-1}$)	λ_{emis} (nm)	Φ_F	τ (ns)	k_r (s^{-1})[a]	k_{nr} (s^{-1})[b]
1	552	23000	565	0.76	8.3	9.2E7	2.9E7
2	561	18000	575	0.70	7.4	9.5E7	4.1E7
3	580	20300	632	0.55	4.7	1.1E8	9.6E7
4	578	34900	621	0.87	4.2	2.0E8	3.1E7
5	551	19700	565	0.77	8.7	8.8E7	2.6E7
6	620	51700	653	0.26	2.2	1.1E8	3.4E8
7	564	18400	585	0.81	8.8	9.2E7	2.1E7
8	567	42600	581	0.68	3.8	1.2E8	8.4E7

[a] Radiative rate of relaxation, and [b] Non-radiative rate of relaxation. Each of these is determined using a combination of the quantum yield of fluorescence and excited state lifetime.

To better understand the trends in electronic structures of these molecules, we performed density functional theory (DFT) and time-dependent density functional theory (TD-DFT) calculations.[43] Their geometries are optimized with the B3LYP functional and the 6-31G+(d,p) basis set, using a polarizable dielectric continuum model for chloroform. The frontier molecular orbitals (FMOs) and vertical excitations are then calculated on these optimized structures with the 6-311+(d,p) basis set. All eight molecules show the aryl rings directly connected to the ethynyl groups highly coplanar with the tetracene unit. Deviations from coplanarity of formally conjugated occur only with crowded moieties: the triarylamines of **3** showing a familiar propeller arrangement of the three aryl rings, and the tetraarylethenes of **8** displaying all four rings skewed from each other, while each maintains coplanarity between the ethynylphenyl and the tetracene core. As summarized in Table 2, the trends in calculated HOMO energies agree with those determined using cyclic voltammetry in CH_2Cl_2, with those molecules bearing conjugated substituents that are considered electron donating (**2**-**4**) showing higher energy HOMO levels than those that have electron withdrawing conjugated units (**5**-**7**).

As summarized in the ESI, the lowest energy singlet excited states computed for all molecules involve primarily or exclusively electronic transition from HOMO to LUMO, and the trend of calculated excited state energies agree with those we measure by UV/vis spectrophotometry in solution. Visual inspection of the FMOs (two examples are in **Figure 3**) only show three clear outliers with respect to their electron distributions, compared to **1**, which shows roughly homogeneous electron distribution across the whole structure for the comparing HOMO and LUMO. Molecules **3** and **4**, which have conjugated amine substituents, show clear donor-acceptor behavior, with substituent phenyl rings having substantially more electron density in their HOMOs than their LUMOs. Benzothiadiazole-containing **6** shows the opposite behavior, with the BTD unit bearing increased electron density in the LUMO. These calculations indicate that the tetracene cores can be substantially polarized by electronic characteristics of the substituent rings that are conjugated through ethynyl linkers.

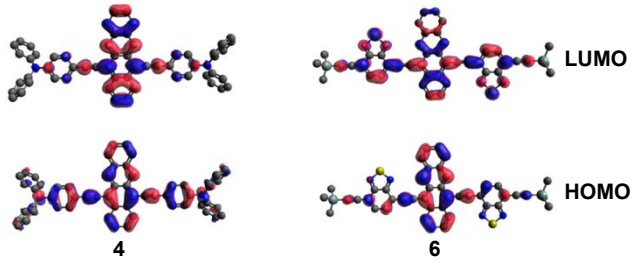

Figure 3. DFT-computed HOMO and LUMO wavefunctions for **4** and **6.**

Kinetics of Oxidation

We also sought to determine the impact of these functional substitutions on the reactivity of these molecules with singlet oxygen ($^1O_2$). We followed the consumption of each tetracene derivative by irradiating an external singlet oxygen photosensitizer, Methylene Blue (**MB**), in the presence of each acene. Under constant irradiation and constant concentration of **MB**, we assume the concentration of $^1O_2$ in the reaction is constant while irradiating, enabling us to use a pseudo first-order kinetic model—each kinetic analysis fits a first-order reaction model well. Thus, we determine the trend in tetracene reactivity quantitatively by comparing the relative rate constants, which we report here in relation to compound **1**.

Table 2. Electrochemical and reactivity parameters of tetracenes **1**-**8**.

	E_{HOMO} (eV)[a]	E_{LUMO} (eV)[b]	k_{rel}[c]	E_{HOMO} (eV), DFT	E_{LUMO} (eV), DFT
1	-5.08	-2.94	1.00 ± 0.02	-5.18	-3.01
2	-5.20	-3.13	1.12 ± 0.04	-5.12	-3.04
3	-4.89	-2.94	4.44 ± 0.15	-4.72	-2.74
4	-4.97	-3.02	1.73 ± 0.23	-4.90	-2.90
5	-5.15	-3.02	0.87 ± 0.05	-5.30	-3.14
6	-5.23	-3.42	0.69 ± 0.06	-5.26	-3.48
7	-5.32	-3.24	0.44 ± 0.02	-5.43	-3.32
8	-5.22	-3.24	1.31 ± 0.13	-5.15	-2.98

[a] CV acquired in CH_2Cl_2. [b] Estimated by adding onset excitation energy and E_{HOMO}. [c] Relative rate constants of oxidation determined in $CHCl_3$, presented as mean values ± standard error of the mean of three replicates.

Figure 4 shows exemplar pseudo first-order kinetic analysis and relative rate constant determination for tetracenes **3** and **7**, while Table 2 contains the relative rate constants for all tetracenes reported here. In general, molecules with higher energy HOMO levels react faster than those with lower energy HOMO levels, as shown in Figure 4b. Therefore, arenes typically considered as electron-donating accelerate the reactions of diethynyltetracenes with $^1O_2$, while electron-withdrawing acenes decelerate these reactions. We note a ten-fold range of rate constants, with the pyrazine-substituted **7** slowest, and the dimethylaniline-substituted **3** reacting ten times faster, indicating that the wide panoply of available aromatic structures substantially impact cycloaddition reactivities of acenes.

Beyond measuring the intrinsic rates of reactivity of these acenes with $^1O_2$, we also examine here the impact of alkyne-spaced electron-donating/withdrawing groups on the bleaching of tetracenes upon direct irradiation. We isolate the 546 nm Hg emission line with a bandpass filter and start each irradiation experiment with the same absorbance value (0.4) at 546 nm. **Figure 5** shows the degradation of each molecule upon irradiation. Surprisingly, all other molecules show a slower degradation rate than **1**. In general, however, there is a reasonable general correlation with observed rate, as **6** and **7** react slowest, and besides **1**, **3** reacts fastest. Here, we suspect that these results are due to a combination of photosensitizing efficiency and intrinsic rate of reaction. For example, **6** having the lowest quantum yield of fluorescence and slowest rate of degradation in this experiment suggests that, at least to some degree, non-radiative decay of the excited state of **6** competes with singlet oxygen photosensitization.

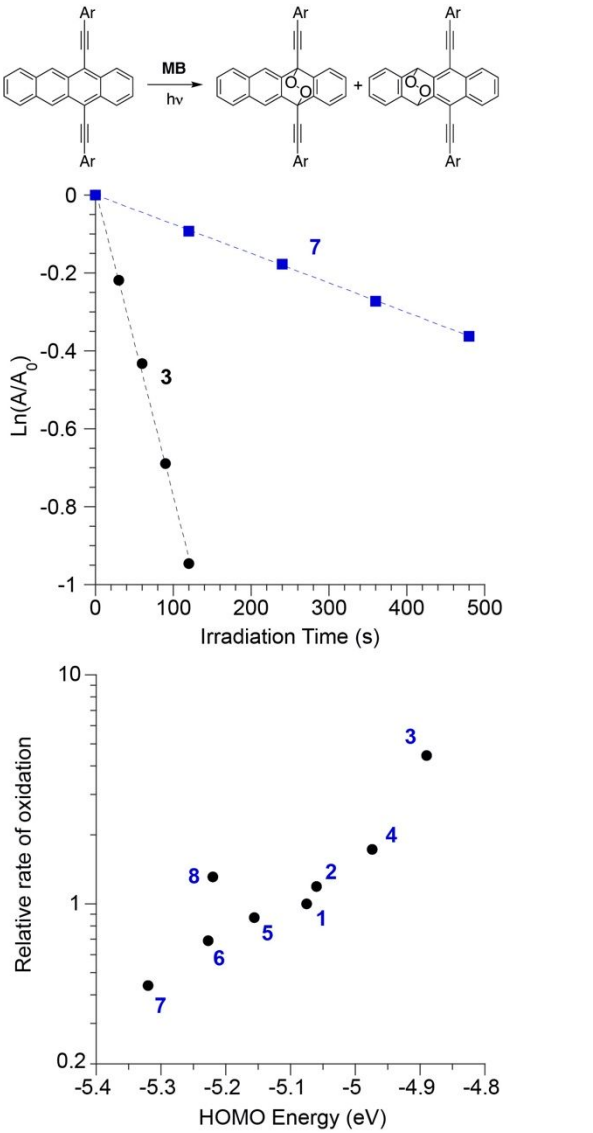

Figure 4. *Top:* Photooxidation reaction scheme. *Middle:* Exemplar pseudo first-order kinetics fit for tetracenes **3** and **7** as a function of irradiation time of **MB**. *Bottom*: Dependence of relative observed rate of oxidation on energy of tetracene HOMO determined by cyclic voltammetry.

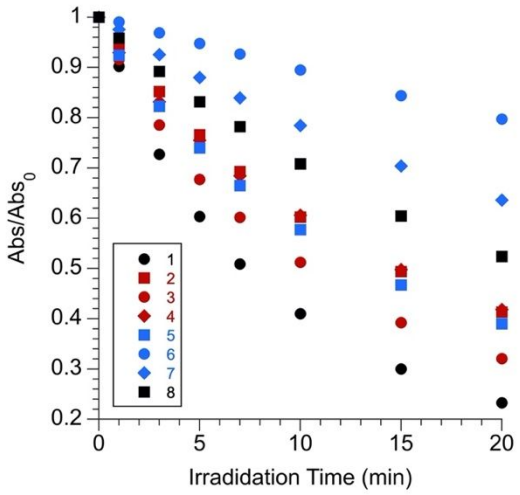

Figure 5. Bleaching of diethynyltetracenes upon direct irradiation at 546 nm.

Ratiometric Responses to $^1O_2$

In addition to the changes in absorbance we use to monitor kinetics, all the molecules show a significant blue-shift in fluorescence upon reacting with singlet oxygen. We attribute this spectroscopic change to the destruction of the conjugated tetracene core. Such changes give these molecules potential for use in of singlet oxygen sensing applications. Among the molecules described here, the more highly conjugated tetracenes **4** and **6** show favorable ratiometric fluorescent signals, with emission peaks highly spectrally separated (140 nm for **4**, and110 nm for **6**) before and after the reaction, while maintaining strong fluorescent intensity (Figure 6).

Given the favorable photophysical and chemical properties of the tetracene derivatives here, we explored the possibility of applying them to a singlet oxygen responsive materials platform based on conjugated polymer nanoparticles (CPNs) dispersed in water. We selected molecule **6** to examine because it has the most red-shifted emission spectrum. Following a nano-precipitation method reported by McNeill group[44-46] and used previously in our group,[10] we doped **6** into a matrix of poly(9,9-dioctylfluorene-*alt*-benzothiadiazole) (**F8BT**) with various weight percentages. **Figure 7** shows the emission of the CPNs with different dopant levels. With 3% (w/w) of dopant, the original emission of **F8BT** is almost fully quenched by energy transfer (ET),[26] with emission emanating primarily from the dopant at 660 nm. Directly irradiating the CPNs generated singlet oxygen, which oxidized **6** and we monitored by fluorescence spectroscopy. Upon irradiation, a 120 nm hypochromic shift occurred, highlighting the application potential of **6** in ratiometric fluorescent singlet oxygen sensing.

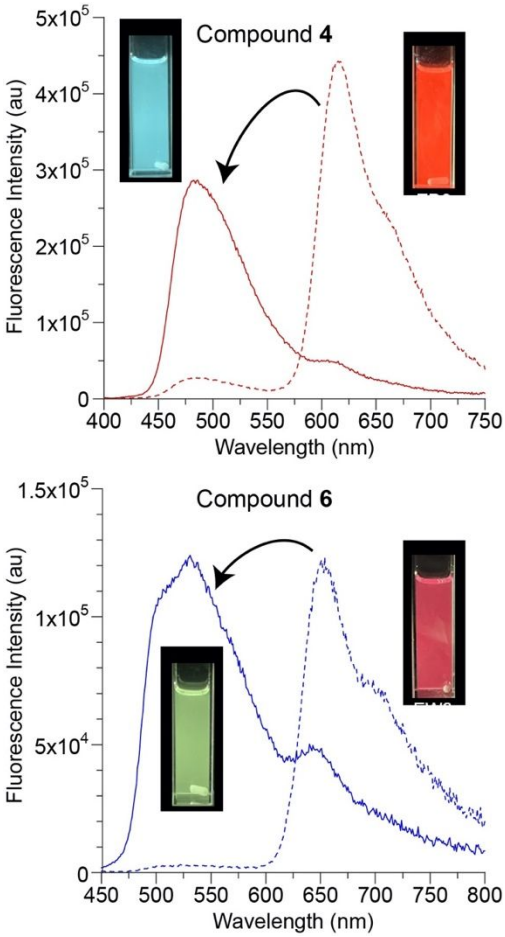

Figure 6. Hypsochromic fluorescent response of tetracenes **4** and **6** to $^1O_2$ in chloroform.

Conclusions

This work therefore expands on the existing understanding of the often-beneficial impact of ethynyl groups on acenes longer than three rings showing that electronic characteristics of groups conjugated to those alkynes can also impact long acenes in substantial ways. Specifically, substituted phenyl groups and especially heteroaromatic arenes offer a wide panoply of design parameter space that can tune optoelectronic properties and photo-oxidation reactivity across a wide range within the diethynyltetracene structural class, yielding tetracenes that show favorable fluorescence behavior in responsive material platforms. Given that tetracenes offer two reactive rings, we anticipate these electronic effects, which here span 90 nm in fluorescence and 10-fold in intrinsic reactivity with $^1O_2$, could be larger in molecules that present one ring that is substantially more reactive than others, such as anthradithiophenes. This work highlights the potential of fully exploring and understanding the chemical space of conjugated materials beyond the portions that are typically thought of as most important.

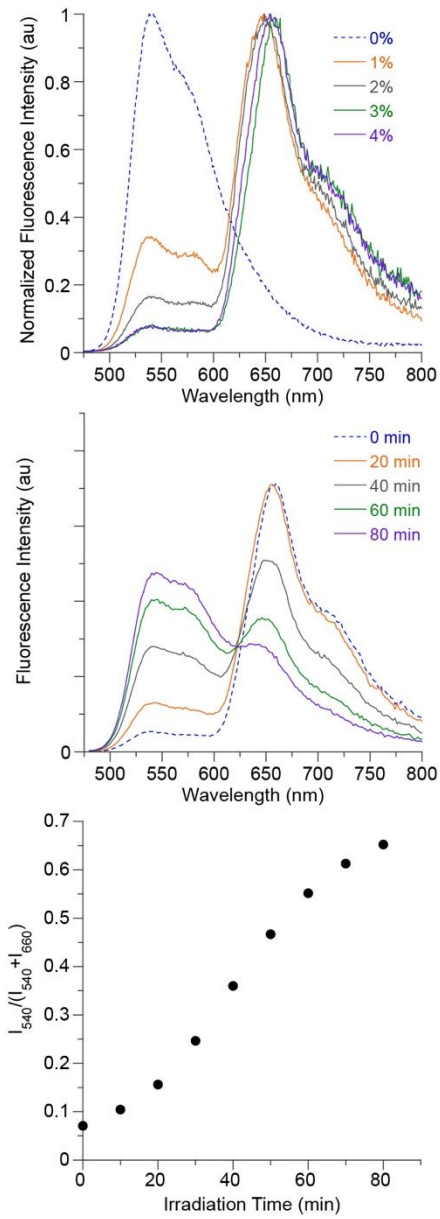

Figure 7. *Top:* Dependence of **F8BT/6** CPN fluorescence on percentage (w/w) of **6** dopant present relative to **F8BT**. *Middle and Bottom*: Response of fluorescence spectrum of 3% **F8BT/6** CPNs to irradiation at 435 nm in water.

Conflicts of interest

There are no conflicts of interest to declare.

Acknowledgements

This work was supported by the National Science Foundation, under award DMR-2003341. Y.Y was supported in part by the U. S. Department of Energy, Basic Energy Sciences, Materials Chemistry Program under Award DE-SC0016423.

Notes and references

1. J. E. Anthony, *Chem. Rev.*, 2006, **106**, 5028-5048.
2. J. E. Anthony, *Angew. Chem. Int. Ed.*, 2008, **47**, 452-483.
3. K. J. Thorley and J. E. Anthony, *Israel Journal of Chemistry*, 2014, **54**, 642-649.
4. C. Tönshoff and H. F. Bettinger, *Chemistry*, 2021, **27**, 3193-3212.
5. S. S. Zade and M. Bendikov, *J. Phys. Org. Chem.*, 2012, **25**, 452-461.
6. J. Van Damme and F. Du Prez, *Prog. Polym. Sci.*, 2018, **82**, 92-119.
7. J. Van Damme, L. Vlaminck, G. Van Assche, B. Van Mele, O. van den Berg and F. Du Prez, *Tetrahedron*, 2016, **72**, 4303-4311.
8. M. C. Paderes, M. Jeffrey Diaz, C. A. Pagtalunan, D. A. Bruzon and G. A. Tapang, *Chem. Asian J.*, 2022, **17**, e202200193.
9. S. Dong, A. Ong and C. Chi, *J. Photochem. Photobiol. C Photochem. Rev.*, 2019, **38**, 27-46.
10. F. Frausto and S. W. Thomas, *ACS Appl. Mater. Interf.*, 2017, **9**, 15768-15775.
11. E. Altinok, F. Frausto and S. W. Thomas, *J. Polym. Sci. Part A Polym. Chem.*, 2016, **54**, 2526-2535.
12. S. W. Thomas, E. Altinok and J. Zhang, *Synlett*, 2016, **27**, 355-368.
13. E. Altınok, Z. C. Smith and S. W. Thomas, *Macromolecules*, 2015, **48**, 6825-6831.
14. J. Zhang, S. Sarrafpour, R. H. Pawle and S. W. Thomas, *Chem. Commun.*, 2011, **47**, 3445-3447.
15. M. Müller, L. Ahrens, V. Brosius, J. Freudenberg and U. H. F. Bunz, *J. Mater. Chem. C*, 2019, **7**, 14011-14034.
16. J. Zhang, R. H. Pawle, T. E. Haas and S. W. Thomas, *Chem. Eur. J.*, 2014, **20**, 5880-5884.
17. R. N. Baral and S. W. Thomas, *J. Org. Chem.*, 2015, **80**, 11086-11091.
18. I. Kaur, W. Jia, R. P. Kopreski, S. Selvarasah, M. R. Dokmeci, C. Pramanik, N. E. McGruer and G. P. Miller, *J. Am. Chem. Soc.*, 2008, **130**, 16274-16286.
19. J. Ly, K. Martin, S. Thomas, M. Yamashita, B. Yu, C. A. Pointer, H. Yamada, K. R. Carter, S. Parkin, L. Zhang, J.-L. Bredas, E. R. Young and A. L. Briseno, *J. Phys. Chem. A*, 2019, **123**, 7558-7566.
20. T. Saegusa, H. Sakai, H. Nagashima, Y. Kobori, N. V. Tkachenko and T. Hasobe, *J. Am. Chem. Soc.*, 2019, **141**, 14720-14727.
21. J. E. Anthony, D. L. Eaton and S. R. Parkin, *Org. Lett.*, 2002, **4**, 15-18.
22. J. Zhang, Z. C. Smith and S. W. Thomas, *J. Org. Chem.*, 2014, **79**, 10081-10093.
23. W. Fudickar and T. Linker, *J. Am. Chem. Soc.*, 2012, **134**, 15071-15082.
24. W. Fudickar and T. Linker, *Chem. Eur. J.*, 2011, **17**, 13661-13664.
25. V. Brega, S. N. Kanari, C. T. Doherty, D. Che, S. A. Sharber and S. W. Thomas, *Chem. Eur. J.*, 2019, **25**, 10400-10407.
26. F. Frausto and S. W. Thomas, *ChemPhotoChem*, 2018, **2**, 632-639.
27. P. J. Hanhela and D. B. Paul, *Aust. J. Chem.*, 1981, **34**, 1701-1717.
28. P. J. Hanhela and D. B. Paul, *Aust. J. Chem.*, 1984, **37**, 553-559.
29. S. N. Sanders, E. Kumarasamy, A. B. Pun, M. L. Steigerwald, M. Y. Sfeir and L. M. Campos, *Angew. Chem. Int. Ed.*, 2016, **55**, 3373-3377.

30. S. N. Sanders, E. Kumarasamy, A. B. Pun, K. Appavoo, M. L. Steigerwald, L. M. Campos and M. Y. Sfeir, *J. Am. Chem. Soc.*, 2016, **138**, 7289-7297.

31. J. Kim, H. T. Teo, Y. Hong, J. Oh, H. Kim, C. Chi and D. Kim, *Angew. Chem. Int. Ed.*, 2020, **59**, 20956-20964.

32. K. J. Fallon, E. M. Churchill, S. N. Sanders, J. Shee, J. L. Weber, R. Meir, S. Jockusch, D. R. Reichman, M. Y. Sfeir, D. N. Congreve and L. M. Campos, *J. Am. Chem. Soc.*, 2020, **142**, 19917-19925.

33. G. He, L. M. Yablon, K. R. Parenti, K. J. Fallon, L. M. Campos and M. Y. Sfeir, *J. Am. Chem. Soc.*, 2022, **144**, 3269-3278.

34. C. B. Dover, J. K. Gallaher, L. Frazer, P. C. Tapping, A. J. Petty, 2nd, M. J. Crossley, J. E. Anthony, T. W. Kee and T. W. Schmidt, *Nat. Chem.*, 2018, **10**, 305-310.

35. N. A. Pace, D. H. Arias, D. B. Granger, S. Christensen, J. E. Anthony and J. C. Johnson, *Chem. Sci.*, 2018, **9**, 3004-3013.

36. S. A. Odom, S. R. Parkin and J. E. Anthony, *Org. Lett.*, 2003, **5**, 4245-4248.

37. M.-A. Tehfe, J. Lalevée, F. Morlet-Savary, B. Graff, N. Blanchard and J.-P. Fouassier, *Macromolecules*, 2012, **45**, 1746-1752.

38. R. Liao, F. Wang, Y. Guo, Y. Han and F. Wang, *J. Am. Chem. Soc.*, 2022, **144**, 9775-9784.

39. Z. Zhao, J. W. Y. Lam and B. Z. Tang, *J. Mater. Chem.*, 2012, **22**, 23726-23740.

40. B. Q. Liu, H. Nie, X. B. Zhou, S. B. Hu, D. X. Luo, D. Y. Gao, J. H. Zou, M. Xu, L. Wang, Z. J. Zhao, A. J. Qin, J. Peng, H. L. Ning, Y. Cao and B. Z. Tang, *Adv. Funct. Mater.*, 2016, **26**, 776-783.

41. F. Effenberger, F. Wuerthner and F. Steybe, *J. Org. Chem.*1995, **60**, 2082-2091.

42. Q. Qiu, P. Xu, Y. Zhu, J. Yu, M. Wei, W. Xi, H. Feng, J. Chen and Z. Qian, *Chem. Eur. J.*, 2019, **25**, 15983-15987.

43. Gaussian 09, Revision D.01, M. J. Frisch, G. W. Trucks, H. B. Schlegel, G. E. Scuseria, M. A. Robb, J. R. Cheeseman, G. Scalmani, V. Barone, G. A. Petersson, H. Nakatsuji, X. Li, M. Caricato, A. Marenich, J. Bloino, B. G. Janesko, R. Gomperts, B. Mennucci, H. P. Hratchian, J. V. Ortiz, A. F. Izmaylov, J. L. Sonnenberg, D. Williams-Young, F. Ding, F. Lipparini, F. Egidi, J. Goings, B. Peng, A. Petrone, T. Henderson, D. Ranasinghe, V. G. Zakrzewski, J. Gao, N. Rega, G. Zheng, W. Liang, M. Hada, M. Ehara, K. Toyota, R. Fukuda, J. Hasegawa, M. Ishida, T. Nakajima, Y. Honda, O. Kitao, H. Nakai, T. Vreven, K. Throssell, J. A. Montgomery, Jr., J. E. Peralta, F. Ogliaro, M. Bearpark, J. J. Heyd, E. Brothers, K. N. Kudin, V. N. Staroverov, T. Keith, R. Kobayashi, J. Normand, K. Raghavachari, A. Rendell, J. C. Burant, S. S. Iyengar, J. Tomasi, M. Cossi, J. M. Millam, M. Klene, C. Adamo, R. Cammi, J. W. Ochterski, R. L. Martin, K. Morokuma, O. Farkas, J. B. Foresman, and D. J. Fox, Gaussian, Inc., Wallingford CT, 2016.

44. C. Wu, C. Szymanski and J. Mcneill, *Langmuir*, 2006, **22**, 2956-2960.

45. Z. Tian, J. Yu, C. Wu, C. Szymanski and J. Mcneill, *Nanoscale*, 2010, **2**, 1999.

46. Y. Jiang and J. McNeill, *Chem. Rev.*, 2017, **117**, 838-859.